Published online 3 July 2011 *Nucleic Acids Research, 2011, Vol. 39, No. 18* ***8237–8247***
doi:10.1093/nar/gkr381

Broad-spectrum aptamer inhibitors of HIV reverse transcriptase closely mimic natural substrates

Mark A. Ditzler[1], Debojit Bose[1,2], Nikolozi Shkriabai[3], Bruno Marchand[1], Stefan G. Sarafianos[1,4,5], Mamuka Kvaratskhelia[3] and Donald H. Burke[1,4,5,*]

[1]Molecular Microbiology and Immunology, University of Missouri, [2]Proteomics and Structural Biology Unit, Institute of Genomics and Integrative Biology, CSIR, Delhi, India, [3]Center for Retrovirus Research and Comprehensive Cancer Center, College of Pharmacy, The Ohio State University, Columbus, OH 43210, USA, [4]Department of Biochemistry, University of Missouri, and [5]Bond Life Sciences Center, University of Missouri, Columbia, MO 65211

Received March 10, 2011; Revised April 27, 2011; Accepted April 29, 2011

ABSTRACT

A detailed understanding of how aptamers recognize biological binding partners is of considerable importance in the development of oligonucleotide therapeutics. For antiviral nucleic acid aptamers, current models predict a correlation between broad-spectrum inhibition of viral proteins and suppression of emerging viral resistance, but there is little understanding of how aptamer structures contribute to recognition specificity. We previously established that two independent single-stranded DNA aptamers, R1T and RT1t49(−5), are potent inhibitors of reverse transcriptases (RTs) from diverse branches of the primate lentiviral family, including HIV-1, HIV-2 and SIV(cpz). In contrast, class 1 RNA pseudoknots, such as aptamer T1.1, are specific for RTs from only a few viral clades. Here, we map the binding interfaces of complexes formed between RT and aptamers R1T, RT1t49(−5) and T1.1, using mass spectrometry-based protein footprinting of RT and hydroxyl radical footprinting of the aptamers. These complementary methods reveal that the broad-spectrum aptamers make contacts throughout the primer-template binding cleft of RT. The double-stranded stems of these aptamers closely mimic natural substrates near the RNase H domain, while their binding within the polymerase domain significantly differs from RT substrates. These results inform our perspective on how sustained, broad-spectrum inhibition of RT can be achieved by aptamers.

INTRODUCTION

Aptamers are small nucleic acids that bind with high affinity to defined molecular targets. *In vitro* selection has identified aptamers for hundreds of different proteins (1–8), including potential therapeutic targets such as VEGF (1,2), factor IXa (3) and human immunodeficiency virus (HIV) reverse transcriptase (RT) (6–14). These aptamers adopt structures with a variety of motifs such as pseudoknots, stem loops, and quadruplexes. The interrelated properties of binding affinity and specificity are governed by the interplay between these structures and the physical nature of aptamer-protein interfaces. Elucidating these interfaces can accelerate preclinical development by guiding optimization of nucleotide sequence and of chemical modifications that increase *in vivo* retention (15,16), cell-type specificity (17,18) and intracellular delivery.

Aptamers' ability to interfere with replication or infection has been demonstrated for HIV (19), hepatitis C virus (20,21) and *Salmonella enterica* (22), among others, leading to significant interest in using these aptamers to study pathogenic mechanisms and for development of novel therapeutics. Eventual use of aptamers in a clinical context can potentially be limited by variation among circulating pathogens and by ongoing evolution during low-level replication. Aptamers that inhibit a broad spectrum of related pathogens are anticipated to be less susceptible to escape mutations that evade inhibition. Knowledge of these aptamer's binding interfaces can aid in improving aptamer design to suppress potential evolution of resistance among viral or bacterial proteins. The present work therefore seeks to define the binding interfaces associated with broad-spectrum inhibition of HIV-1 RT.

Among the single-stranded (ss) DNA aptamers selected to bind the HIV-1 RT, four of the previously identified families include double-stranded stems with either recessed 3′- or 5′-ends (7). Those with recessed 3′-ends (families I and II) can act as substrates for DNA polymerization and be extended by RT in the presence of dNTPs (7). Extension weakens affinity of the complex, making these aptamers poor inhibitors. In contrast, aptamers with

*To whom correspondence should be addressed. Tel: +1 573 884 1316; Fax: +1 573 884 9676; Email: burkedh@missouri.edu

recessed 5′-ends (families III and VI) cannot act as substrates, and several of these have proven to be potent inhibitors of RT's polymerase and RNase H activities (7,9,23,24). The RNA aptamers to the RT of HIV-1 include a variety of pseudoknot and stem loop structures (6,8,13).

Here we focus on three aptamers—RT1t49(−5), R1T and T1.1—each of which binds HIV-1 RT with K_d values in the low nanomolar range and acts as a potent inhibitor. RT1t49(−5) and R1T exhibit broad-spectrum inhibition of diverse RTs from HIV-1, HIV-2 and SIV strains. Aptamer T1.1 is more specific and only inhibits RT from HIV-1 subtypes B and C (9,23,25). The DNA aptamers RT1t49(−5) and R1T are truncated aptamers derived from structural families III and VI, respectively, and each has a recessed 5′-end (7,9,26). The RNA aptamer T1.1 is a 'class 1' pseudoknot, which was the RNA motif most commonly encountered among the sequences isolated from *in vitro* selection experiments (6,13). RT from HIV-1 sub-type B strain BH10 was the target in each of these selections.

Mutational analysis of RT1t49(−5) and R1T revealed little sensitivity to the sequences of their double-stranded stems as long as base pairing was retained (9,26). However, there are essential sequence requirements for the 3′ overhangs. For R1T and the family VI aptamers from which it was derived, the 3′ overhangs are G rich and capable of forming a quadruplex structure. This quadruplex has been verified by circular dichroism and mutational analysis and is necessary for RT inhibition (9). Similarly, the 19 nt 3′ overhang of aptamer RT1t49 could be shortened by five nucleotides (hence the designation '−5') to generate aptamer RT1t49(−5), but further truncations and various point mutations of this overhang seriously compromised RT inhibition (26). These observations demonstrate that the potent inhibition observed for these aptamers is not merely a consequence of having dsDNA with a recessed 5′-end. However, there have been no systematic studies of the determinants of broad-spectrum inhibition.

In this work, we define the binding interfaces of RT-aptamer complexes using mass spectrometry (MS)-based protein footprinting and hydroxyl radical footprinting of the aptamers. The former approach monitors surface accessibility of lysines in free RT versus the RT-aptamer complex. For hydroxyl radical footprinting, the DNA is cleaved by radicals generated from reduction of hydrogen peroxide by Fe(II). The hydroxyl radicals are generated both by Fe(II) in solution and by Fe(II) bound specifically to RT. Therefore, the radical induced cleavage of aptamers reflects either the solvent accessibility of the aptamers or their proximity to a metal ion binding site in RT. We find that the broad-spectrum inhibitors contact a similar surface of HIV-1 RT as that protected by the natural substrates and that both R1T and RT1t49(−5) bind with similar orientations relative to RT. Our data support models in which both of these aptamers contact the RNase H domain with a double-stranded stem and contact the polymerase domain with their respective 3′ structures.

MATERIALS AND METHODS

RT and oligonucleotides

RT from HIV-1 strain HXB2 (group M, subtype B), which is nearly identical to that of BH10, was expressed in *Escherichia coli* strain BL21(DE3) and purified as previously described (27). DNA oligonucleotides were synthesized by Integrated DNA Technologies Inc. (www.idtdna.com). The RNA aptamer T1.1 was transcribed *in vitro* from a partially double-stranded DNA (dsDNA) template with a T7 promoter by incubation in buffer containing 120 mM HEPES–KOH, pH 7.5, 30 mM $MgCl_2$, 2 mM spermidine, 40 mM DTT, 0.01% Triton X-100 (v/v) with 4 mM each of NTPs, and T7 RNA polymerase for 3 h at 37°C. Full-length transcripts were isolated using denaturing PAGE (20% acrylamide, 8 M Urea). The DNA duplex substrate used for footprinting containing a 5-nt 3′ overhang was obtained by annealing two oligos: 5′-ATGCATCGGCGCTCGAACAGGGACTGT G-3′ and 5′-CACAGTCCCTGTTCGAGCGCCGA-3′. Aptamer sequences are given in Figures 1, 5B and Supplementary Figure S1, with the exception of CE4.3, for which the full sequence was used: 5′-AGCAGCACA GAGGTCAGATGGCAGGTTTCGACGTACAATGC TATGGAGGCTTTATGATCGCCTATGCGTGCTAC CGTGAA-3′ (11). For all the experiments nucleic acids were refolded by heating to 90°C for 1 min and then allowing to cool to ambient temperature for at least 10 min before use.

DNA dependent DNA polymerization assays

Primer extension reactions utilized a [^{32}P]-5′-end labeled 18 nt DNA primer and a 40 nt DNA template corresponding to the viral tRNA primer-binding sequence (PBS) and U5 segments of HIV-1 strain HXB2 were used. Aptamer-RT complexes were pre-assembled in buffer (50 mM HEPES–NaOH pH 7.5, 50 mM NaCl, 6 mM $MgCl_2$) with 200 nM aptamer, 30 nM RT and 0.4 mM dNTPs for 5 min. Polymerization reactions were then initiated by adding pre-annealed 30 nM primer and 60 nM template (final concentrations). After 20 min at 37°C, reactions were quenched by addition of 2 volumes (20 µl) of gel-loading buffer (95% formamide with 0.01% bromophenol blue) and analyzed by high-voltage denaturing polyacrylamide gel electrophoresis. Band intensities were quantified using Multigauge software to determine the fraction of primer extended to full length.

MS-based footprinting of RT-aptamer complexes

Protein–nucleic acid complexes were preformed by mixing 10 µM aptamer or DNA substrate with 5 µM RT in a 10 µl reaction mix of 50 mM HEPES-NaOH (pH 7.5), 50 mM NaCl, 6 mM $MgCl_2$. Complexes were then modified by adding 500 µM Sulfo-*N*-hydroxysuccinimidobiotin (Sulfo-NHS-biotin) (Pierce). Sulfo-NHS-biotin reacts preferentially with primary amines on proteins, resulting in covalent addition of a biotin molecule (226.30 Da) to lysine and the concomitant release of Sulfo-NHS. After incubation at 37°C for 30 min, biotinylation reactions were quenched with 10 mM lysine. Samples were then

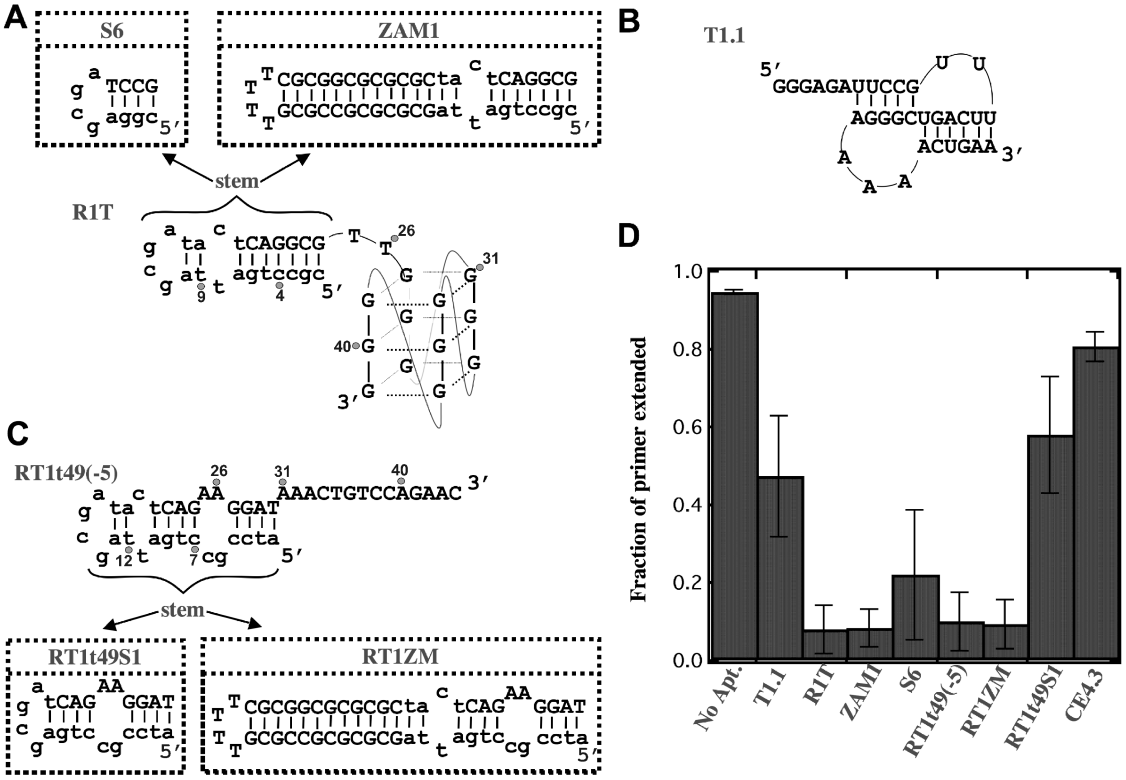

Figure 1. Secondary structures of aptamers used in this work for MS-based protein footprinting of RT-aptamer complexes. (**A**) The stem of R1T is shortened or lengthened to generate aptamers S6 and ZAM1, respectively. The single T residues in the intra-quadruplex loops of each of the shared quadruplex domains are shown as curved lines. (**B**) Secondary structures T1.1 and (**C**) RT1t49(−5); the stem of RT1t49(−5) is shortened or lengthened to generate aptamers RT1t49S1 and RT1ZM, respectively. (**D**) Inhibition of HIV-1 RT DNA dependent DNA polymerization activity by various aptamers. The fraction of primer (30 nM) extended by RT (30 nM) in the presence of aptamer (200 nM), after a 20 min extension time is shown.

treated with 100 mM iodoacetamide for 45 min to cap cysteines to prevent disulfide formation. After separating the mixture by denaturing SDS–PAGE, the p66 and p51 subunits were visualized by Coomassie blue stain, excised and processed separately. Gel slices were destained in 50% acetonitrile overnight, washed twice with ddH_2O, dehydrated with 100% acetonitrile, vacuum desiccated, and finally exposed to 1 μg of trypsin in 50 mM NH_4HCO_3 buffer (pH 7.8) at ambient temperature for >16 h. The supernatant from this digestion was recovered and subjected to mass spectrometric analysis. Mass spectra were recorded using matrix-assisted laser desorption ionization-time of flight (MALDI-TOF) techniques. MALDI-TOF experiments were performed with the Kratos Axima-CFR instrument (Shimadzu Scientific Instruments) using α-cyano-4-hydroxy-cinnamic acid as a matrix. For accurate quantitative analysis of the biotinylated peptide peaks, the intensities of all MS peptide peaks during the entire run, as well as at least two adjacent unmodified RT peptide peaks, were considered as controls.

Structure probing by hydroxyl radicals

Hydroxyl radical footprinting reactions were performed using methods similar to those previously described for mapping nucleic acid-RT binding interactions (26,28,29). [^{32}P]-5′-end labeled DNA aptamer (~60 000 c.p.m.) was incubated in 50 mM Tris–HCl (pH 7.5), 50 mM NaCl, 5 mM $MgCl_2$ in the presence or absence of 300 nM HIV-1 RT and equilibrated for 10 min at room temperature in a total volume of 17 μl at the bottom of a 1.7 ml centrifuge tube. The hydroxyl radical footprinting solution was generated by placing 1 μl of a freshly prepared Fe(II)-EDTA [or Fe(II)] solution (400 μM), 1 μl hydrogen peroxide solution (0.6% freshly diluted from a 30% stock), and 1 μl of ascorbate solution (40 mM) as three separate drops on the side of the tube. The reaction was initiated by simultaneously combining the three 1 μl drops with the DNA aptamer solution by briefly spinning the tube in a centrifuge. Final concentrations of 20 μM Fe(II), 40 μM EDTA and 1 mM ascorbate were used unless otherwise noted. The reactions were quenched by addition of stop solution (2.5 mM thiourea) after 2 min incubation.

RESULTS

The broad spectrum DNA inhibitors R1T and RT1t49(−5) contact an extended functional surface on RT

We assayed inhibition of RT-catalyzed primer extension using the following eight aptamers of potential interest under the conditions used in our MS-based protein footprinting: R1T and two derivatives (Figure 1A), RT1t49(−5) and two derivatives (Figure 1B), the RNA

pseudoknot T1.1 (Figure 1C) and ssDNA aptamer CE4.3 derived from capillary electrophoresis. Consistent with prior studies (9,26), inhibition was strongest for RT1t49(−5), R1T, and their respective stem-extended variants RT1ZM and ZAM1. Inhibition was also observed, to lesser degrees, for the stem-shortened variants RT1t49S1 and S6 and for the RNA aptamer T1.1. Aptamer CE4.3, which binds RT with very high affinity under very low-salt conditions (11), exhibited little or no inhibition of RT under the same polymerization conditions as the other aptamers (Figure 1D) and exhibited little or no binding at modest salt concentrations in independent assays (data not shown). Subsequent work therefore focused on the aptamers whose structures are shown in Figure 1.

Surface-exposed lysine side chains of RT react with sulfo-NHS-biotin and are readily identified by MS analysis of tryptic peptides of the isolated subunits (30). Peaks in the spectra that arise from RT fragments with biotinylated lysines are identified based on the predicted mass of the fragment plus the mass of covalently attached biotin (226 Da). In the presence of nucleic acid, the intensities of peaks from several biotinylated fragments are significantly diminished relative to the majority of peaks in the spectrum; this reflects protection of the corresponding lysines from modification due likely to their interactions with the nucleic acid. These changes in the modification pattern define the chemical modification footprint for the nucleoprotein complex, which can then be interpreted in the context of available crystal structures of RT. Using this approach, we determined surface topologies of several RT-aptamer complexes by mapping their modification patterns onto a crystal structure of RT bound to a dsDNA substrate (Figure 2). Protected and unprotected lysines are summarized in Table 1.

Broad-spectrum aptamers R1T, RT1t49(−5) and their variants all protect lysines across an extended surface of RT along the substrate binding cleft. The protection pattern for a dsDNA substrate is identical to that of aptamer RT1t49(−5). RNA aptamer T1.1 protects lysine residues within a portion of the substrate-binding cleft, but the footprint is restricted to the center of that cleft, as expected from the low-resolution crystal structure of this complex (31). Overall, fewer lysines are protected by T1.1 than by the DNA aptamers or by the dsDNA substrate. Specifically, T1.1 does not protect the RNase H domain residue K540 in the p66 subunit or K390 in p51 subunit. Both of these are protected in all of the DNA-RT complexes. Thus, T1.1 appears to make fewer contacts with RT than do the DNA aptamers or the dsDNA substrate.

Protections in the polymerase domain further differentiate aptamer-RT complexes

Double-stranded DNA substrates sit between the thumb and fingers subdomains of RT. In the substrate-free state,

Table 1. Biotinylation pattern of RT, and RT-nucleic acid complexes

	p66			p51		
Amino acid	dsDNA substrate, RT1t49(−5) and RT1t49S1	R1T, S6 and ZAM1	T1.1	dsDNA substrate, RT1t49(−5) and RT1t49S1	R1T, S6 and ZAM1	T1.1
K22	NA	NA	NA	–	–	–
K30	+	–	+	NA	NA	NA
K70	+	+	+	+	+	+
K73	+	+	+	+	+	+
K82	–	–	–	+	+	+
K201	+	+	+	+	+	+
K219	+	+	+	+	+	+
K263	NA	NA	NA	+	+	+
K281	–	–	–	+	+	+
K287	–	–	–	+	+	+
K353	–	+	–	+	+	+
K366	–	–	–	+	+	+
K390	NA	NA	NA	–	–	+
K451	–	–	–	NP	NP	NP
K454	+	+	+	NP	NP	NP
K540	–	–	+	NP	NP	NP
K550	+	+	+	NP	NP	NP

Lysines readily modified by Sulfo-NHS-biotin in the absence of nucleic acid are listed. –, lysines significantly protected from biotinylation in the presence of the corresponding nucleic acid; +, lysines that are still modified in the presence of nucleic acid; NA, lysines not amenable to biotinylation in the absence of nucleic acid for one of the subunits; NP, lysines representing the RNase H domain that are not present in p51.

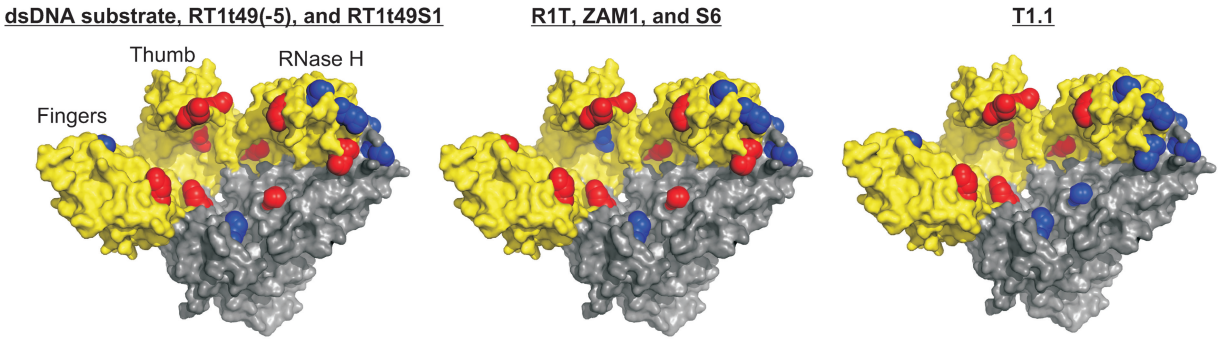

Figure 2. The protected lysines mapped onto a crystal structure of HIV-1 RT (PDB 3KK2); the dsDNA substrate present in the crystal structure is not shown. Lysines protected from modification by the nucleic acid are shown as red spheres, and those not protected are shown as blue spheres. Lysines for which no signal was observed in either the absence or presence of nucleic acid are not explicitly shown. The same protection pattern is conferred by the dsDNA substrate and the aptamers RT1t49(−5) and RT1t49S1. Aptamers R1T, ZAM1 and S6 share a distinct protection pattern. A third protection pattern is observed for T1.1.

the thumb fluctuates between an open conformation similar to that of the substrate-bound state and a more prevalent closed state in which thumb swings down to contact the fingers directly (32–35). The identical protection patterns for RT1t49(−5) and a dsDNA substrate suggest that this aptamer occupies a very similar surface as native dsDNA substrates, which includes the cleft between the thumb and fingers in the thumb-open conformation. Mutations N255D and N265D were previously identified through an *in situ* colony-screening assay for their abilities to confer biochemical resistance to RT1t49 (36), which is nearly identical to RT1t49(−5). These two amino acids within alpha helix H (αH) are much more accessible in the open conformation than in the closed conformation, providing further support for the RT being in an open conformation in its complexes with RT1t49 and with the truncated RT1t49(−5).

Protection patterns mapped onto a crystal structure of RT bound to a dsDNA substrate show that the pattern conferred by aptamer R1T is distinguished from that of aptamers RT1t49(−5) and T1.1 by the protection pattern of K30 in the fingers subdomain and K353 at the base of the thumb subdomain (Figures 2 and 3). In the complex with R1T, K30 is protected while K353 is not protected, and the same pattern is observed for complexes with the R1T variants (ZAM1 and S6); however, this protection pattern is reversed for complexes with RT1t49(−5), and the RT1t49(−5) variant RT1t49S1. Thus, these differences in protection pattern do not vary with stem length but rather with the identity of the 3′ overhang structures. We have previously shown that binding of R1T to RT requires two structural modules (a stem domain and a quadruplex domain) and a physical connection between them, with little constraint on the chemical nature of that connection (9). Therefore, the gap in protection of K353 may reflect the presence of two semi-independent binding sites on the RT, with one on either side of K353. This interpretation is further supported by the experiments described in the following sections.

In the complex of RT with RNA pseudoknot T1.1, the thumb domain adopts the closed conformation, both in crystal structures (31) and in solution (34). The protection pattern of RT in the complex with T1.1 in solution is essentially consistent with the crystal structure of the T1.1-RT complex (Figure 4). K353, for example, is protected by T1.1 and is close to the aptamer in the crystal structure, while K30 is not protected and is not in the proximity of the aptamer. Some lysines show unexpected protection patterns. Lysine K390 in the p51 subunit is in the vicinity of T1.1 (the β carbon is only 5 Å from the aptamer backbone in the crystal structure), but it is not protected. In this case, the side chain (which is not

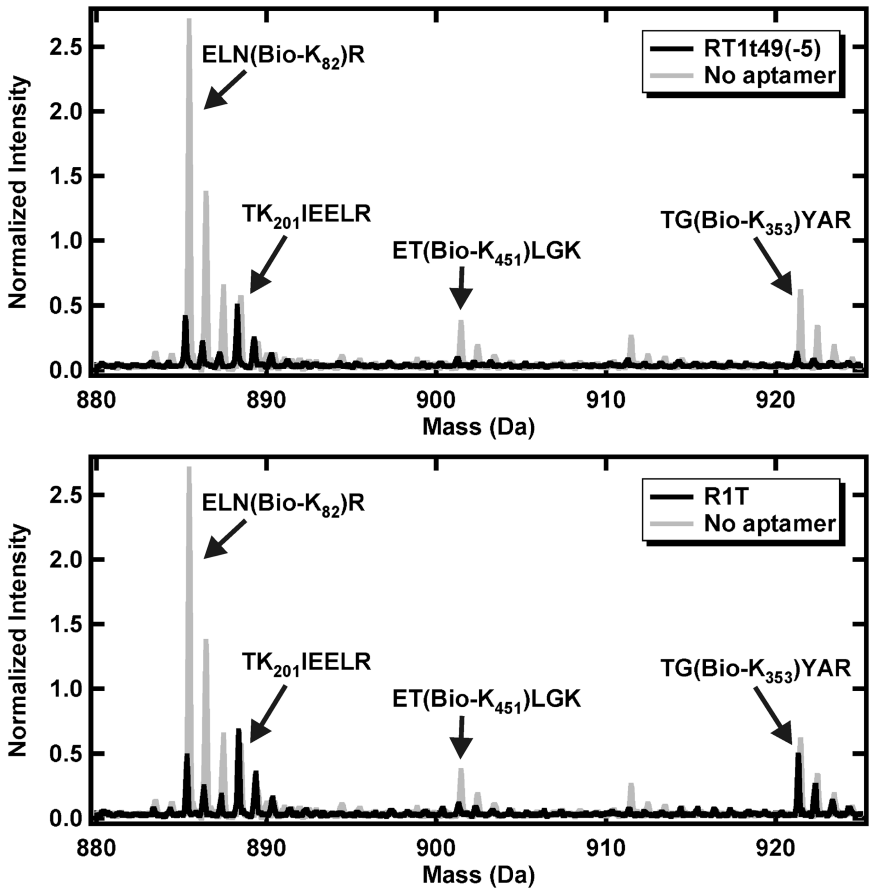

Figure 3. MALDI-TOF data illustrating similarities and differences between the abilities of RT1t49(−5) and R1T to protect specific lysines. This part of the spectra shows that K82 and K451 are protected by both aptamers, while K353 is only protected by RT1t49(−5) and not by R1T.

resolved in the 4.8 Å structure) may be directed away from T1.1. Conversely, lysines K287 and K451 in the p66 subunit are protected despite being distant from T1.1 (β carbon is >10 Å from the aptamer backbone). This protection of K287 and K451 may arise from additional side chain interactions that are not resolved in the co-crystal structure.

DNA inhibitors R1T and RT1t49(−5) both exhibit hypersensitivity to hydroxyl radical cleavage within their stem domains

Hydroxyl radical mediated cleavage of dsDNA bound to RT can be used to map the position of the DNA relative to the RNase H active site (28,29). Fe(II) replaces Mg(II) within the active sites of RT, where it reacts with hydrogen peroxide to generate a hydroxyl radical locally (26,28). Fe(II) in solution can also generate free radicals that cleave DNA based on solvent accessibility, and that can be used to determine protected surfaces of DNA bound to protein (37,38). Cleavage mediated by the site-specifically bound Fe(II) is eliminated upon chelation by EDTA, whereas cleavage mediated by Fe(II) in solution is largely unaffected by EDTA. Additionally, cleavage mediated by the site-specifically bound Fe(II) can be eliminated by the RT mutation E478Q (29), which has been shown to disrupt metal binding in the RNase H active site (28).

Hydroxyl radical footprinting of aptamer R1T in complex with RT reveals a hypersensitive cleavage site immediately 5′ of its GNRA tetra loop between T9 and A10 (Figures 1A and 5A and Supplementary Figure S1). This hypersensitive cleavage is lost when RT has the mutation E478Q. Aside from this one hypersensitive site, the remainder of the cleavage pattern is identical for wild-type RT and the E478Q mutant. For example, they are both characterized in part by protection from cleavage at positions 18 and 19 in the stem (Figure 5A). Furthermore, the hypersensitive cleavage site of R1T is enhanced by removing EDTA from the reaction (Figure 5A, inset). These observations are consistent with hypersensitive cleavage arising from local generation

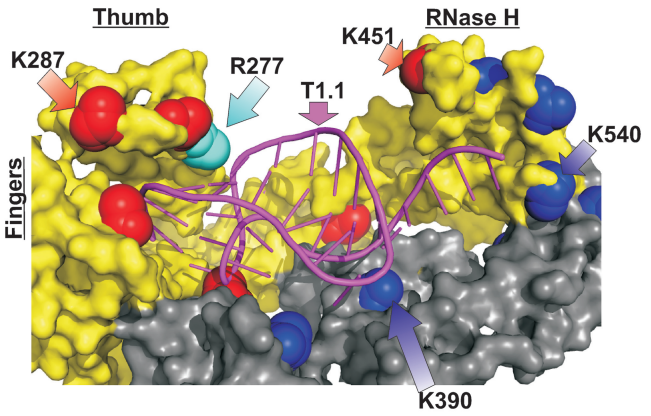

Figure 4. The crystal structure of T1.1 in complex with RT is largely consistent with the protein footprinting pattern (side chains are not resolved). Protected and unprotected lysines are colored as in Figure 2. R277, which is critical to recognition of T1.1 (25), is also indicated (cyan).

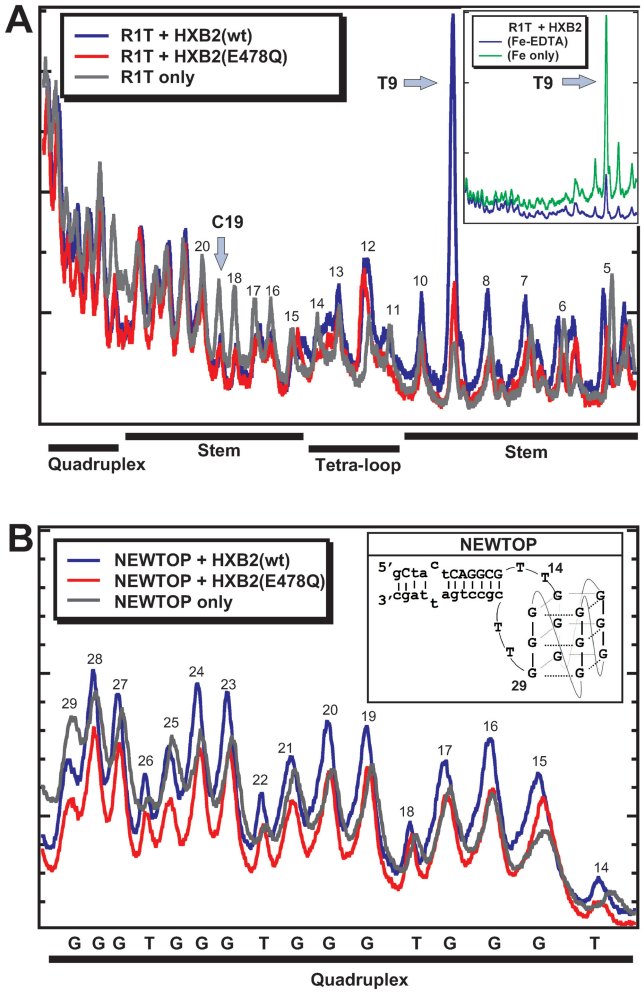

Figure 5. Hydroxyl radical cleavage of aptamers bound to RT. The patterns of cleavage from representative hydroxyl radical digestions are shown. (**A**) R1T is subject to hyper-sensitive cleavage at position T9 when in complex with wt HXB2 RT but not when it is in complex with the E478Q mutant. Hypersensitive cleavage at position 9 is enhanced in the absence of EDTA (inset), which competes with RT for free Fe(II). (**B**) R1T variant Newtop shows a lack of a hypersensitive cleavage in its quadruplex. The secondary structure of Newtop is shown as inset.

of free radicals by Fe(II) bound to the RNase H active site, as observed previously with substrates of RT (28,29). These data provide clear evidence that the backbone of aptamer R1T between T9 and A10 is positioned at the RNase H active site.

To further define the features of R1T that determine its positioning on RT, footprinting was applied to ZAM1 and three additional R1T variants: MAD1 (in which the stem is fully paired with canonical base-pairs), Acut (a topological variant in which the 5′-end is moved to the middle of the quadruplex) and Newtop (a topological variant in which the 5′- and 3′-ends are moved to within the original tetra-loop) (Supplementary Figure S1). For ZAM1 and MAD1, hypersensitivity is in the same position as R1T. For Acut, the cleavage is between T18 and A19, which are equivalent to positions T9 and A10 in R1T. For Newtop, the equivalent position is not resolved

on the footprinting gel. These results indicate that the quadruplex is fixed relative to the RT and that the position of the tetraloop relative to RT varies with the length of the stem. The quadruplex domain of Newtop, which is clearly resolved in these assays, does not exhibit site-specific hypersensitivity to hydroxyl radical cleavage; instead, only minor alterations in cleavage intensities are observed throughout (Figure 5B). The quadruplex domain thus does not exhibit any evidence of specific interaction with the RNase H active site. In addition, the cleavage pattern of the quadruplex exhibits a decreased sensitivity to cleavage after each T in the $(TGGG)_4$ quadruplex. Periodicity in the cleavage pattern is observed in both the absence and presence of protein, consistent with this sequence adopting a three-tiered quadruplex that is retained upon binding of the RT.

Our previous footprinting of RT1t49(−5) in complex with RT revealed a hypersensitive cleavage site immediately 5′ of the GNRA tetra-loop in stem 1 (26). In the present work, we observe similar hypersensitive cleavage by hydroxyl radicals in the RT1t49(−5) variant RT1ZM (Figures 1A and 6, and Supplementary Figure S1). Hypersensitive cleavage of RT1ZM is retained for the wild-type HXB2 RT, but it is lost in the presence of the E478Q mutation (Figure 6). Furthermore, hypersensitive cleavage of the aptamer at this position is enhanced by removing EDTA from the reaction (Figure 6, inset). These observations are consistent with hypersensitive cleavage arising from local generation of free radicals by Fe(II) bound to the RNase H active site, as observed previously with substrates of RT (28,29). These data provide clear evidence that the backbone of aptamer RT1ZM between T12 and A13 is positioned at the RNase H active site. One additional cleavage site with sensitivity to the E478Q mutation is observed between positions 17 and 18, but it is neither hypersensitive nor EDTA dependent (Figure 5A). Importantly, the locations of the hypersensitive sites in RT1t49(−5) and RT1ZM are governed by their distances from their respective 5′-ends of the aptamers and not the distances from their tetra-loops, which are positioned at a variable distance according to the lengths of the stems (Figure 1A). Anchoring the hypersensitive sites relative to the RNase H active site fixes the distances to the 3′ overhang.

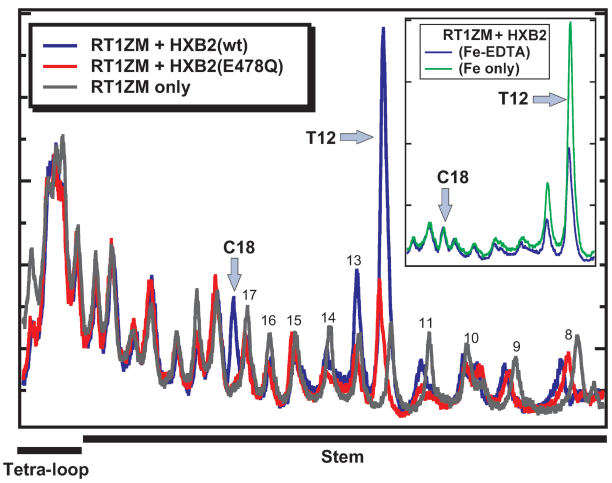

Figure 6. Hydroxyl radical cleavage of the RT1t49(−5) variant RT1ZM bound to RT. The patterns of cleavage from representative hydroxyl radical digestions are shown. RT1ZM is subject to hypersensitive cleavage at position T12 when in complex with wt HXB2 RT but not when it is in complex with the RNase H defective E478Q mutant. Hypersensitive cleavage at position 12 is enhanced in the absence of EDTA (inset), which competes with RT for free Fe(II).

In our previously reported hydroxyl radical footprinting experiments with RT1t49(−5), hypersensitive cleavage of RT1t49(−5) was not altered by the E478Q mutation. This stands in apparent contrast to the E478Q dependence described here for the RT1t49(−5) variant RT1ZM. However, the hydroxyl radical footprinting experiments described here were carried out at a 20-fold lower Fe(II) concentration [20 μM Fe(II), 40 μM EDTA] than used previously (26,28). Under conditions similar to those used in our previous study [200 μM Fe(II), 400 μM EDTA] RT1ZM also displays hypersensitive cleavage by hydroxyl radicals that is unaltered by the E478Q mutation (Supplementary Figure S2). Thus, our current footprinting data reveal that hydroxyl radical cleavage of aptamers bound to the E478Q mutant of RT is dependent upon Fe(II) concentration. Specifically, they show that elevated Fe(II) concentrations can obscure the impact of the E478Q mutation on hypersensitive cleavage of nucleic acids bound to RT. The result is consistent with E478Q retaining an affinity for metal ions that is greatly diminished but not entirely eliminated. Alternative mechanisms could also be involved, given the previous observation that hydroxyl radical induced cleavage of RT itself was clearly reduced for the E478Q mutant at a relatively high concentration of Fe(II) [400 μM Fe(II), 800 μM EDTA] (28).

DISCUSSION

Interaction model for RT1t49(−5)

Aptamers selected to bind HIV-1 RT differ in structure from natural substrates and from each other. The broad-spectrum inhibitors share a double-stranded stem feature with recessed 5′-ends. Substrates for polymerization-independent RNase H assays also carry recessed 5′-ends; however, those substrates are DNA–RNA hybrids while the aptamers are DNA only and possess variable but essential elements within the 3′ overhangs (39). Despite the differences between the RT inhibitors and substrates, both the data presented here and prior characterization suggest highly similar binding by RT1t49(−5) and substrates of RT. These findings are consistent with previous mutational and footprinting studies (26,36), which suggested that contacts between the aptamer and RT lie both within and adjacent to surfaces contacted by the native substrates. Specifically, the prior model suggested that the stem of RT1t49(−5) occupies the primer/template-binding cleft, and the structural unit present in the 3′ overhang was thought to interact with the back side of the fingers or thumb subdomains (26). However, there are important differences between the previous model and our data presented here.

We observe RNase H active site mediated hydroxyl radical cleavage between positions T12 and A13 of the RT1t49(−5) stem. The 12 bp of a dsDNA substrate extending from the RNase H active site toward the polymerase active site in the substrate bound crystal structure (PDB 3KK2) just reach K353 (Figure 7). Using this portion of the dsDNA substrate as a model for the RT1t49(−5) stem, the stem is just long enough to provide the observed protection of K353 from NHS-biotin modification. In contrast to our previous model (26), this positioning of the RT1t49(−5) stem (based on the RNase H active site mediated hydroxyl radical cleavage presented here) places the 5′-end of the stem next to N265 and the 3′-end of the stem does not reach N255 (Figure 7). N255 is most proximal to the dsDNA substrates 13 bp away from the RNase H active site and N265 is in close proximity to dsDNA substrates 12 bp away from the RNase H active site. This suggests that resistance is conferred by mutations at these sites by disrupting contacts with the 3′ overhang and 5′ terminus of RT1t49(−5), respectively. Additionally, our MS data demonstrate a lack of protection of lysines K219, K70 and K73 which are positioned on the far side of the polymerization active site and represent a likely boundary for the aptamer-RT interface. In summary, our current data confine the overall RT1t49(−5)-RT binding surface to that of the dsDNA substrate.

Interaction model for R1T

In addition to the R1T family of quadruplex aptamers, G-rich sequences capable of forming quadruplexes are found within multiple aptamers selected to bind to the RNase H domain of RT (10,14). Among these, quadruplexes 93del and $(GGGT)_4$ bind HIV-1 integrase, which is in the same structural superfamily as RNase H. These observations imply that the quadruplex domains of R1T and related aptamers bind the RNase H domain of RT. However, our data argue otherwise.

For R1T, the RNase H mediated hydroxyl radical cleavage occurs between position T9 and A10 of the stem. Similarly, hypersensitivity sites are observed at equivalent positions for R1T variants. The 9 bp of a dsDNA substrate extending from the RNase H active site toward the polymerase active site in the substrate bound crystal structure (PDB 3KK2) falls short of reaching K353 (Figure 8). Using this portion of the dsDNA substrate as a model for the R1T stem, the stem is not long enough to contact K353, which is in fact not protected from modification by NHS-biotin by R1T (Figures 2 and 3). This positioning of the stem suggests the 3′ module of R1T resides on the far side of K353 within the polymerase domain, between the fingers and thumb subdomains, connected to the 3′-end of the stem through a flexible linker. Mutational analysis and CD spectroscopy of R1T has shown that for this aptamer the 3′ module forms a three-tiered parallel quadruplex (9). High-resolution structures do not exist for R1T, but structures do exist for other three-tiered parallel quadruplexes such as the quadruplex derived from the myc promoter (PDB 1XAV) which has a similar sequence $(TGAG_3TG_3TAG_3TG_3TA)$ (40). Given the dimensions of parallel, three-tiered quadruplexes for which structures have been determined (40,41), visual inspection shows that such a quadruplex could be reasonably well accommodated by the cleft between the thumb and fingers subdomains upon minor adjustments to residues in the RT (Figure 8 and Supplementary Figure S3).

Comparison with RT-aptamer interactions for RNA pseudoknot T1.1

The footprint of the RNA pseudoknot T1.1 in complex with RT in solution covers a smaller surface area than does that of the DNA aptamers. Importantly, the interface differs significantly between T1.1 and RT substrates, as evidenced by lack of protection at position K540 in p66 and K390 in p51 reported here, by the low-resolution

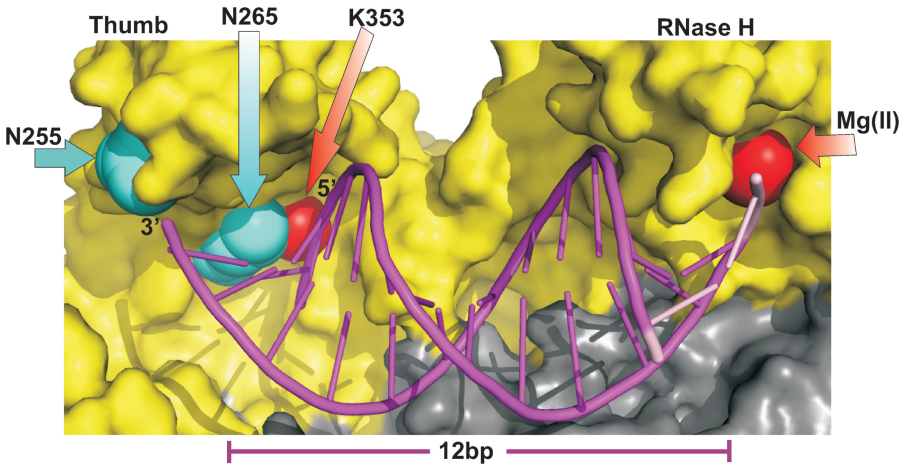

Figure 7. A crystal structure of RT in complex with a dsDNA substrate (PDB 3KK2); only a portion of the dsDNA substrate that extends 12 bp from the RNase H active site is shown to approximate the position of the stem of RT1t49(−5), the positions equivalent to the 5′- and 3′-ends of the stem are indicated. The figure illustrates how the stem of RT1t49(−5) can protect K353. Residues N255 and N265 that play a role in recognition of RT1t49 are shown (cyan). N255 is not contacted by the nucleotides in the 12 bp shown, and N265 is in proximity to the 5′-end of the portion of the template stand that is shown.

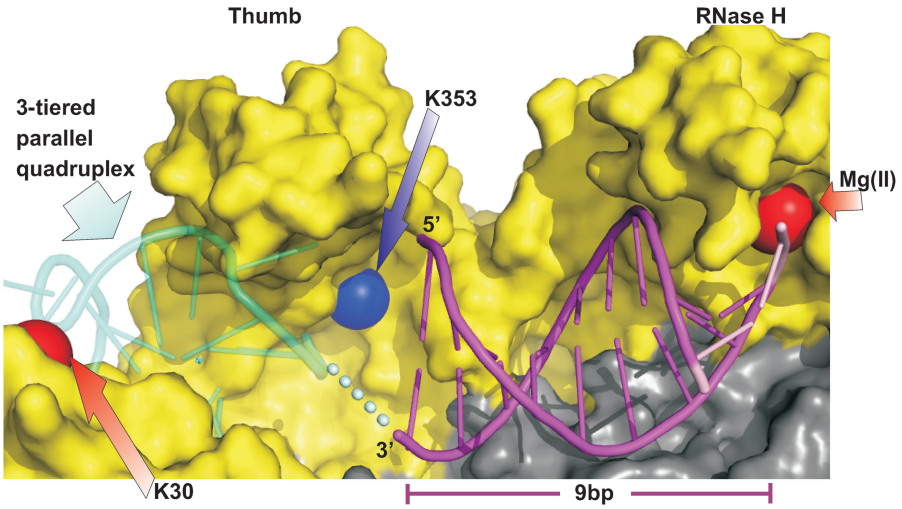

Figure 8. Crystal structure of RT in complex with a dsDNA substrate (PDB 3KK2); only a portion of the dsDNA substrate that extends 9 bp from the RNase H active site is shown to approximate the position of the stem of R1T, the positions equivalent to the 5′- and 3′-ends of the stem are indicated. A three-tiered parallel quadruplex derived from the myc promoter is also shown to illustrate one of several possible binding modes in which R1T binds along the substrate binding cleft while leaving K353 accessible to NHS-biotin modification.

crystal structure (31), and by solution studies of thumb conformational dynamics (34). The dissimilarities between T1.1 binding and that of natural substrates creates opportunities for natural RT amino acid sequence variation to disrupt binding of the aptamer without loss of fitness for the virus. For example, while RT's from HIV strains with R277 (such as HXB2 and 98CN009) were strongly inhibited by T1.1 and related family 1 pseudoknots, a single R277K point mutation conferred resistance to the T1.1 aptamer. Both arginine and lysine are commonly encountered at position 277 among circulating HIV-1, HIV-2 and SIV strains. Interestingly, other RNA aptamers were much less sensitive to the identity of position 277 (25), potentially signaling that broad-spectrum RNA aptamers could also be generated.

Mechanisms of broad-spectrum inhibition

Our data suggest that the broad-spectrum inhibition of diverse primate lentiviral RTs by R1T, RT1t49(−5) and their variants is likely to arise from a combination of at least the following three factors. First, the aptamers make numerous contacts with the enzyme over a large surface area. MS-based footprinting reveals an extended binding interface between RT and two independent classes of DNA aptamers. Second, MS-based footprinting and observations from hydroxyl radical cleavage reveal that binding by these aptamers is remarkably similar to binding by natural nucleic acid substrates, with major contacts residing within the interface formed between RT and its natural substrates. For the quadruplex aptamer R1T and its analogs, an apparent exception is K30, which is protected by the aptamers but not by the dsDNA substrate; however, the tRNA:vRNA primer-template complex was previously shown to protect K30 from modification by NHS-biotin (30); therefore, K30 is within the interface that RT uses to bind its various natural substrates. To the extent that inhibitors and natural substrates share a binding interface, mutations that disrupt binding of the inhibitor can be expected to diminish affinity for the replicating viral genome and compromise viral fitness (9,23,36), with the caveat that even with a shared interface, there may be differences in some of the atomic-level contacts with RT. This conjecture is supported by observations with RT1t49, for which the RT mutations N255D and N265D confer biochemical resistance both individually and in combination, but are defective *in vivo* due to diminished affinity for the natural substrates (36). Third, both classes of broad-spectrum aptamers appear to bind RT in the thumb-and-fingers-open conformation, as indicated by the overall similarity of the protection pattern to that of dsDNA or tRNA:vRNA primer-template complex, which bind to RT in the open conformation. This is further evidenced for RT1t49(−5) by the location of resistance mutations N255D and N265D, which are buried and inaccessible in the closed conformation.

In sum, our data support interaction models in which both the RT1t49 family and the R1T quadruplex family interact at two separate sites on the RT. The respective 3′ overhangs are between the fingers and thumb subdomains, and the double-stranded stems reach across the RNase H active site. These DNA aptamers act as broad-spectrum inhibitors of RT by competing with substrates for RT while remaining inert to the enzymatic activities of RT. They accomplish this by binding in a substrate-like manner away from the polymerization active site, while their positioning in the polymerase active site significantly differs from RT substrates.

SUPPLEMENTARY DATA

Supplementary Data are available at NAR Online.

FUNDING

Funding for open access charge: NIH grant 5R01AI074389 (to D.H.B.) and AI062520 and AI077341 (to M.K.).

Conflict of interest statement. None declared.

REFERENCES

1. Jellinek,D., Green,L.S., Bell,C. and Janjic,N. (1994) Inhibition of receptor binding by high-affinity RNA ligands to vascular endothelial growth factor. *Biochemistry*, **33**, 10450–10456.
2. Ng,E.W., Shima,D.T., Calias,P., Cunningham,E.T. Jr, Guyer,D.R. and Adamis,A.P. (2006) Pegaptanib, a targeted anti-VEGF aptamer for ocular vascular disease. *Nat. Rev. Drug Discov.*, **5**, 123–132.
3. Dyke,C.K., Steinhubl,S.R., Kleiman,N.S., Cannon,R.O., Aberle,L.G., Lin,M., Myles,S.K., Melloni,C., Harrington,R.A., Alexander,J.H. *et al.* (2006) First-in-human experience of an antidote-controlled anticoagulant using RNA aptamer technology: a phase 1a pharmacodynamic evaluation of a drug-antidote pair for the controlled regulation of factor IXa activity. *Circulation*, **114**, 2490–2497.
4. Keefe,A.D. and Schaub,R.G. (2008) Aptamers as candidate therapeutics for cardiovascular indications. *Curr. Opin. Pharmacol.*, **8**, 147–152.
5. de Soultrait,V.R., Lozach,P.Y., Altmeyer,R., Tarrago-Litvak,L., Litvak,S. and Andreola,M.L. (2002) DNA aptamers derived from HIV-1 RNase H inhibitors are strong anti-integrase agents. *J. Mol. Biol.*, **324**, 195–203.
6. Tuerk,C., MacDougal,S. and Gold,L. (1992) RNA pseudoknots that inhibit human immunodeficiency virus type 1 reverse transcriptase. *Proc. Natl Acad. Sci. USA*, **89**, 6988–6992.
7. Schneider,D.J., Feigon,J., Hostomsky,Z. and Gold,L. (1995) High-affinity ssDNA inhibitors of the reverse transcriptase of type 1 human immunodeficiency virus. *Biochemistry*, **34**, 9599–9610.
8. Li,N., Wang,Y., Pothukuchy,A., Syrett,A., Husain,N., Gopalakrisha,S., Kosaraju,P. and Ellington,A.D. (2008) Aptamers that recognize drug-resistant HIV-1 reverse transcriptase. *Nucleic Acids Res.*, **36**, 6739–6751.
9. Michalowski,D., Chitima-Matsiga,R., Held,D.M. and Burke,D.H. (2008) Novel bimodular DNA aptamers with guanosine quadruplexes inhibit phylogenetically diverse HIV-1 reverse transcriptases. *Nucleic Acids Res.*, **36**, 7124–7135.
10. Somasunderam,A., Ferguson,M.R., Rojo,D.R., Thiviyanathan,V., Li,X., O'Brien,W.A. and Gorenstein,D.G. (2005) Combinatorial selection, inhibition, and antiviral activity of DNA thioaptamers targeting the RNase H domain of HIV-1 reverse transcriptase. *Biochemistry*, **44**, 10388–10395.
11. Mosing,R.K., Mendonsa,S.D. and Bowser,M.T. (2005) Capillary electrophoresis-SELEX selection of aptamers with affinity for HIV-1 reverse transcriptase. *Anal. Chem.*, **77**, 6107–6112.
12. Hannoush,R.N., Carriero,S., Min,K.L. and Damha,M.J. (2004) Selective inhibition of HIV-1 reverse transcriptase (HIV-1 RT) RNase H by small RNA hairpins and dumbbells. *Chembiochem.*, **5**, 527–533.
13. Burke,D.H., Scates,L., Andrews,K. and Gold,L. (1996) Bent pseudoknots and novel RNA inhibitors of type 1 human immunodeficiency virus (HIV-1) reverse transcriptase. *J. Mol. Biol.*, **264**, 650–666.
14. Andreola,M.L., Pileur,F., Calmels,C., Ventura,M., Tarrago-Litvak,L., Toulme,J.J. and Litvak,S. (2001) DNA aptamers selected against the HIV-1 RNase H display in vitro antiviral activity. *Biochemistry*, **40**, 10087–10094.
15. Boomer,R.M., Lewis,S.D., Healy,J.M., Kurz,M., Wilson,C. and McCauley,T.G. (2005) Conjugation to polyethylene glycol polymer promotes aptamer biodistribution to healthy and inflamed tissues. *Oligonucleotides*, **15**, 183–195.
16. Wilson,C. and Keefe,A.D. (2006) Building oligonucleotide therapeutics using non-natural chemistries. *Curr. Opin. Chem. Biol.*, **10**, 607–614.
17. McNamara,J.O. II, Andrechek,E.R., Wang,Y., Viles,K.D., Rempel,R.E., Gilboa,E., Sullenger,B.A. and Giangrande,P.H. (2006) Cell type-specific delivery of siRNAs with aptamer-siRNA chimeras. *Nat. Biotechnol.*, **24**, 1005–1015.
18. Zhou,J., Li,H., Li,S., Zaia,J. and Rossi,J.J. (2008) Novel dual inhibitory function aptamer-siRNA delivery system for HIV-1 therapy. *Mol. Ther.*, **16**, 1481–1489.
19. Joshi,P. and Prasad,V.R. (2002) Potent inhibition of human immunodeficiency virus type 1 replication by template analog reverse transcriptase inhibitors derived by SELEX (systematic evolution of ligands by exponential enrichment). *J. Virol.*, **76**, 6545–6557.
20. Chen,F., Hu,Y., Li,D., Chen,H. and Zhang,X.L. (2009) CS-SELEX generates high-affinity ssDNA aptamers as molecular probes for hepatitis C virus envelope glycoprotein E2. *PLoS One*, **4**, e8142.
21. Bellecave,P., Cazenave,C., Rumi,J., Staedel,C., Cosnefroy,O., Andreola,M.L., Ventura,M., Tarrago-Litvak,L. and Astier-Gin,T. (2008) Inhibition of hepatitis C virus (HCV) RNA polymerase by DNA aptamers: mechanism of inhibition of in vitro RNA synthesis and effect on HCV-infected cells. *Antimicrob. Agents Chemother.*, **52**, 2097–2110.
22. Pan,Q., Zhang,X.L., Wu,H.Y., He,P.W., Wang,F., Zhang,M.S., Hu,J.M., Xia,B. and Wu,J. (2005) Aptamers that preferentially bind type IVB pili and inhibit human monocytic-cell invasion by *Salmonella enterica* serovar typhi. *Antimicrob. Agents Chemother.*, **49**, 4052–4060.
23. Kissel,J.D., Held,D.M., Hardy,R.W. and Burke,D.H. (2007) Single-stranded DNA aptamer RT1t49 inhibits RT polymerase and RNase H functions of HIV type 1, HIV type 2, and SIVCPZ RTs. *AIDS Res. Hum. Retroviruses*, **23**, 699–708.
24. Fisher,T.S., Joshi,P. and Prasad,V.R. (2005) HIV-1 reverse transcriptase mutations that confer decreased in vitro susceptibility to anti-RT DNA aptamer RT1t49 confer cross resistance to other anti-RT aptamers but not to standard RT inhibitors. *AIDS Res. Ther.*, **2**, 8.
25. Held,D.M., Kissel,J.D., Thacker,S.J., Michalowski,D., Saran,D., Ji,J., Hardy,R.W., Rossi,J.J. and Burke,D.H. (2007) Cross-clade inhibition of recombinant human immunodeficiency virus type 1 (HIV-1), HIV-2, and simian immunodeficiency virus SIVcpz reverse transcriptases by RNA pseudoknot aptamers. *J. Virol.*, **81**, 5375–5384.
26. Kissel,J.D., Held,D.M., Hardy,R.W. and Burke,D.H. (2007) Active site binding and sequence requirements for inhibition of HIV-1 reverse transcriptase by the RT1 family of single-stranded DNA aptamers. *Nucleic Acids Res.*, **35**, 5039–5050.
27. Michailidis,E., Marchand,B., Kodama,E.N., Singh,K., Matsuoka,M., Kirby,K.A., Ryan,E.M., Sawani,A.M., Nagy,E., Ashida,N. *et al.* (2009) Mechanism of inhibition of HIV-1 reverse transcriptase by 4'-Ethynyl-2-fluoro-2'-deoxyadenosine triphosphate, a translocation-defective reverse transcriptase inhibitor. *J. Biol. Chem.*, **284**, 35681–35691.
28. Gotte,M., Maier,G., Gross,H.J. and Heumann,H. (1998) Localization of the active site of HIV-1 reverse transcriptase-associated RNase H domain on a DNA template using site-specific generated hydroxyl radicals. *J. Biol. Chem.*, **273**, 10139–10146.
29. Metzger,W., Hermann,T., Schatz,O., Le Grice,S.F. and Heumann,H. (1993) Hydroxyl radical footprint analysis of human immunodeficiency virus reverse transcriptase-template.primer complexes. *Proc. Natl Acad. Sci. USA*, **90**, 5909–5913.
30. Kvaratskhelia,M., Miller,J.T., Budihas,S.R., Pannell,L.K. and Le Grice,S.F. (2002) Identification of specific HIV-1 reverse transcriptase contacts to the viral RNA:tRNA complex by mass spectrometry and a primary amine selective reagent. *Proc. Natl Acad. Sci. USA*, **99**, 15988–15993.
31. Jaeger,J., Restle,T. and Steitz,T.A. (1998) The structure of HIV-1 reverse transcriptase complexed with an RNA pseudoknot inhibitor. *EMBO J.*, **17**, 4535–4542.
32. Rodgers,D.W., Gamblin,S.J., Harris,B.A., Ray,S., Culp,J.S., Hellmig,B., Woolf,D.J., Debouck,C. and Harrison,S.C. (1995) The

structure of unliganded reverse transcriptase from the human immunodeficiency virus type 1. *Proc. Natl Acad. Sci. USA*, **92**, 1222–1226.
33. Jacobo-Molina,A., Ding,J., Nanni,R.G., Clark,A.D. Jr, Lu,X., Tantillo,C., Williams,R.L., Kamer,G., Ferris,A.L., Clark,P. *et al.* (1993) Crystal structure of human immunodeficiency virus type 1 reverse transcriptase complexed with double-stranded DNA at 3.0 A resolution shows bent DNA. *Proc. Natl Acad. Sci. USA*, **90**, 6320–6324.
34. Kensch,O., Restle,T., Wohrl,B.M., Goody,R.S. and Steinhoff,H.J. (2000) Temperature-dependent equilibrium between the open and closed conformation of the p66 subunit of HIV-1 reverse transcriptase revealed by site-directed spin labelling. *J. Mol. Biol.*, **301**, 1029–1039.
35. Seckler,J.M., Howard,K.J., Barkley,M.D. and Wintrode,P.L. (2009) Solution structural dynamics of HIV-1 reverse transcriptase heterodimer. *Biochemistry*, **48**, 7646–7655.
36. Fisher,T.S., Joshi,P. and Prasad,V.R. (2002) Mutations that confer resistance to template-analog inhibitors of human immunodeficiency virus (HIV) type 1 reverse transcriptase lead to severe defects in HIV replication. *J. Virol.*, **76**, 4068–4072.
37. Tullius,T.D. and Dombroski,B.A. (1986) Hydroxyl radical 'footprinting': high-resolution information about DNA-protein contacts and application to lambda repressor and Cro protein. *Proc. Natl Acad. Sci. USA*, **83**, 5469–5473.
38. Balasubramanian,B., Pogozelski,W.K. and Tullius,T.D. (1998) DNA strand breaking by the hydroxyl radical is governed by the accessible surface areas of the hydrogen atoms of the DNA backbone. *Proc. Natl Acad. Sci. USA*, **95**, 9738–9743.
39. Palaniappan,C., Fuentes,G.M., Rodriguez-Rodriguez,L., Fay,P.J. and Bambara,R.A. (1996) Helix structure and ends of RNA/DNA hybrids direct the cleavage specificity of HIV-1 reverse transcriptase RNase H. *J. Biol. Chem.*, **271**, 2063–2070.
40. Ambrus,A., Chen,D., Dai,J., Jones,R.A. and Yang,D. (2005) Solution structure of the biologically relevant G-quadruplex element in the human c-MYC promoter. Implications for G-quadruplex stabilization. *Biochemistry*, **44**, 2048–2058.
41. Burge,S., Parkinson,G.N., Hazel,P., Todd,A.K. and Neidle,S. (2006) Quadruplex DNA: sequence, topology and structure. *Nucleic Acids Res.*, **34**, 5402–5415.